Superlattices and Microstructures 125 (2019) 247–255

Contents lists available at ScienceDirect

Superlattices and Microstructures

journal homepage: www.elsevier.com/locate/superlattices

TM plasmonic modes in a multilayer graphene-dielectric structure

J. Madrigal-Melchor[a,*], J.S. Pérez-Huerta[a], J.R. Suárez-López[a], I. Rodríguez-Vargas[a], D. Ariza-Flores[b]

[a] Unidad Académica de Física, Universidad Autónoma de Zacatecas, Calzada Solidaridad Esquina Paseo a la Bufa s/n, CP 98060, Mexico
[b] CONACYT-Instituto de Investigación en Comunicación Óptica, Universidad Autónoma de San Luis Potosí, Av. Karakorum 1470, Lomas 4a sección, San Luis Potosí, SLP 78210, Mexico

ARTICLE INFO

Keywords:
Graphene
Plasmons on surfaces and interfaces
Transversal magnetic polarization
Attenuated total reflection
Optical properties of multilayers

ABSTRACT

Optical and electronic properties of multilayer systems have been extensively studied in the last years due to its potential applications in high-performance optoelectronic and photonic devices. In particular, the role of plasmonic modes is critical in such systems leading to improvements in solar cells efficiency, detection of biosensors, Raman signal enhancement, among others. In this work, we study the plasmonic modes in a multilayer system composed of graphene layers embedded within dielectric materials. The dispersion relation of plasmonic modes is obtained by calculating the poles of reflectivity using the transfer matrix method. We show the attenuated total reflection spectra for a multilayer graphene-dielectric structure, and determine the optimum distance between the prism and the multilayer system for detecting graphene plasmons in the Otto configuration. Additional to the well-known plasmonics bands, when we consider the interband and intraband contribution of graphene's conductivity, and large wavevectors parallel to graphene's plane, all plasmonic bands have an asymptotic behavior. Besides, an upper mode emerges. Finally, it is important to highlight that the number of branches in the plasmonic relation dispersion depend on the number of graphene sheets.

1. Introduction

Plasmonics studies the interaction between electromagnetic radiation and the conduction electrons at a metallic interface. As a branch of nanophotonics, this field has a great interest because it takes advantage of the manipulation, control, and coupling of light at subwavelength dimensions, enhancing the electromagnetic field confinement and also breaking the Abbe limit of diffraction [1–3].

Plasmons have been studied for decades; the first studies about plasmons came in late 1890 and early 1900 with the works of Sommerfeld [4], Zenneck [5] and Wood [6], who studied the interaction between light and metallic media. On the other hand, it is well known that collective excitation of free charge in metallic surfaces, i.e., surface plasmons (SP), can be coupled with the electromagnetic radiation as a surface plasmon polariton (SPP), and play a key role in a broad spectrum of science, ranging from physics and material science to biology and medicine [2,7,8], and references therein. The term plasmon was coined by Ritchie in 1957 [9] and since then it has been extensively studied due to its optical and electrical properties which allow to have diverse applications as waveguides sources, near-field optics, data storage devices, solar cells, surface-enhancement Raman spectroscopy (SERS), chemical sensors and biosensors, see Ref. [2] and references therein. Moreover, it is well known that a multilayer structure of metallic films

* Corresponding author.
E-mail address: jmadrigal.melchor@fisica.uaz.edu.mx (J. Madrigal-Melchor).
URL: http://fisica.uaz.edu.mx/jmadrigal.melchor (J. Madrigal-Melchor).

https://doi.org/10.1016/j.spmi.2018.11.015
Received 15 September 2018; Received in revised form 8 November 2018; Accepted 19 November 2018
Available online 23 November 2018
0749-6036/

embedded within dielectric materials, has a number of plasmon branches in its dispersion relation equal to the number of metallic interfaces of the lattice [3].

The possibility of supporting plasmons in graphene has been investigated since 2006 by different research groups in several works [10–47], where they study and discuss models for optical conductivity of graphene, as well as numerical and analytic calculations for graphene structures embedded in different kind of materials. Experimentally, people have reported several investigations of the SPP interaction phenomena for different systems and applications [16,19,30,38,40,43,45,48]. For example, S. Huang et al., studied the plasmonic modes in the terahertz and mid-infrared region and discuss its localization and propagation. Additionally, they introduce two experimental techniques: absorption spectroscopy and s-SNOM imaging, for detecting plasmons [45]. Xiao et al., report a review work where they discuss the excitation of graphene plasmon polaritons, electron-phonon interactions in graphene on polar substrates, and tunable graphene plasmonics [43]. Jamalpoor et al., introduce a method for coupling light into graphene plasmonic modes, which consists of the use of nonlinear optics process [49]. Sreekanth et al., reported the fabrication of a graphene-based Bragg grating and demonstrate the excitation of surface electromagnetic waves in the periodic structure using the prism coupling technique [48]. On other hand, Jablan et al. and Grigorenko et al., make an extensive discussion over graphene plasmon properties [19,30].

It is important to emphasize three features of graphene which permit us to consider it as an excellent 2D material candidate for supporting plasmons and use it for different applications. Firstly, we know that the carrier mobility in graphene is high as compared to other materials, which implicate low loss in comparison with traditional support plasmons materials. Secondly, graphene conductivity is tunable, by controlling the Fermi level using electrostatic gating or chemical doping [10,32,50]. Finally, graphene plasmons can show very strong light spatial confinement with in-plane propagation distances above 100 times the surface plasmon wavelength [17].

In particular, the research group headed by Bludov [31] has studied the plasmonic modes both for TM and TE polarizations for one and two doped sheets of graphene, showing the dispersion relation for his structure only in the far infra-red region. On the other hand, in many works the authors refer to both intraband and interband contributions in graphene conductivity in their theoretical section, however, in the numerical calculations, the results only show the intraband contribution, i.e., Drude-like conductivity is only taken into account. It is important to highlight that the TE mode cannot be supported in a metallic-dielectric interface.

In this paper, we obtain and analyze numerically the dispersion relation for a graphene-dielectric multilayer system, which consists of N encrusted graphene layers between $N+1$ dielectrics, i.e., dielectric-graphene-dielectric structure. As can be expected, we found that the number of plasmonic branches corresponds to the number of graphene sheets in the system. A significant difference between our work and another graphene multilayer structures is that they only report systems with maximum two graphene sheets in the TeraHertz and far-infrared regions and never show results for the interband contribution, where we found an upper mode for two o more graphene sheets [19,27,31]. For one and two graphene sheets, we show the analytic relation dispersion, numerical calculations of Attenuated Total Reflection (ATR) spectra and we get the optimal distance between coupling prism with the multilayer system to detect the surface polariton plasmons in the Otto configuration. Furthermore, we found that the plasmonic mode branches tend to an asymptotic value of frequency ω_{spp}, in the non-retarder limit for intraband contribution despite the number of graphene sheets. We found that for two graphene sheets or more, the dispersion relation shows an upper mode for high frequency, which is associated to the interband transition which, to our knowledge, it has not been reported before in the literature. For this high mode and in the case of two graphene sheets, we demonstrate its asymptotic behavior derived from the analytic dispersion relation, and for more graphene sheets is obtained via numerical calculations.

2. Theoretical model

In order to study the propagation of the electromagnetic waves in a layered media, we implemented a calculation method based in the scheme of transfer matrix, (see Pochi Yeh and Markos [51,52]). As a graphene sheet is embedded between two dielectric media, the corresponding boundary conditions for any interface are the continuity of the tangential electric field $(\vec{E}_j - \vec{E}_{j+1}) \times \hat{n} = 0$, and the discontinuity of the tangential magnetic field $(\vec{H}_j - \vec{H}_{j+1}) \times \hat{n} = \vec{J} \times \hat{n}$, where $\hat{n}$ is the normal vector of graphene plane and $\vec{J}$ is the surface current density. Furthermore, we employ the Ohm's law $\vec{J} = \sigma\vec{E}$ and we use the isotropic and local optical conductivity of graphene proposed by Falkovsky in the regime $\mu_g \gg k_B T$, where the random-phase approximation is assumed, which considers the intraband and interband transitions [53] as $\sigma = \sigma_{intra} + \sigma_{inter}$, where

$$\sigma_{intra}(\omega) = \frac{ie^2|\mu_g|}{\pi\hbar(\hbar\omega + i\hbar\Gamma)}, \tag{1}$$

$$\sigma_{inter}(\omega) = \frac{e^2}{4\hbar}\left[\Theta(\hbar\omega - 2\mu_g) + \frac{i}{2\pi}\ln\left(\frac{\left(\hbar\omega - 2\mu_g\right)^2}{\left(\hbar\omega + 2\mu_g\right)^2}\right)\right],$$

where ω is the frequency of light, e is the elementary charge, μ_g is the chemical potential, $\hbar$ is the Planck constant over 2π, Γ is the collision frequency and Θ the Heaviside function. Through this model, we obtained the reflection spectra, as well as the plasmonic dispersion relation.

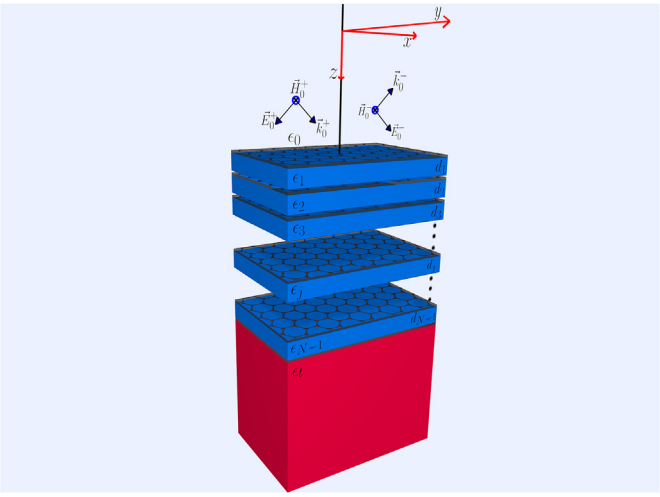

Fig. 1. Schematics of a multilayer graphene-dielectric system over a semi-infinite dielectric medium, for N graphene sheets embedded in different dielectric media. Arrows correspond to the incoming and reflected plane waves (TM) that impinges on the multilayer surface. The dielectric permittivities are represented by ε_j, with respective thicknesses of d_j.

2.1. Transfer matrix method

The transfer matrix method is very useful to calculate the propagation of different kind of waves, such as electromagnetic, acoustic, massive electrons, Dirac electrons waves, through multilayer systems [51,52]. In this paper, we consider harmonic plane waves with transverse magnetic polarization (TM), where the electric and magnetic fields are written as

$$\vec{E_j} = (E_{jx}, 0, E_{jz}), \quad \text{and} \quad \vec{H_j} = (0, H_{jy}, 0). \tag{2}$$

This electromagnetic field configuration and the proposed graphene-dielectric multilayer system are shown in Fig. 1, which consists on N encrusted graphene layers between $N-1$ different dielectrics, with relative permittivity ε_j of medium $j = 1,2,3, \ldots, N$.

The corresponding magnetic field for dielectric media j can be written as:

$$\vec{H_j} = \left[H_j^+ e^{ik_{jz}z} + H_j^- e^{-ik_{jz}z}\right] e^{iq_x x}\,\hat{j}\,, \tag{3}$$

and it is related to the electric field in j-th media by

$$\vec{H_j} = \frac{c}{\omega\mu_j}\vec{k_j} \times \vec{E_j}\,, \tag{4}$$

where $\mu_j = 1$ is the magnetic permeability for non magnetic media j, and k_{jz} is given by

$$k_{jz} = \sqrt{\omega^2/c^2\varepsilon_j - q_x^2} = i\kappa_{jz}. \tag{5}$$

Applying the corresponding boundary conditions on the different interfaces, we obtain the relation between magnetic fields for the incident and transmitting media in the form of

$$\begin{pmatrix} H_0^+ \\ H_0^- \end{pmatrix} = D_0^{-1}[\Pi_{j=1}^{N-1} G_j D_j P_j D_j^{-1}] G_N D_t \begin{pmatrix} H_t^+ \\ 0 \end{pmatrix}, \tag{6}$$

where

$$D_j = \begin{pmatrix} 1 & 1 \\ -\frac{k_{jz}}{\varepsilon_j} & \frac{k_{jz}}{\varepsilon_j} \end{pmatrix}, \qquad P_j = \begin{pmatrix} e^{-ik_{jz}d_j} & 0 \\ 0 & e^{ik_{jz}d_j} \end{pmatrix}, \tag{7}$$

where d_j is the physical thickness of j-th dielectric slab. Subscripts $j = 0$ and t correspond to incident and transmission media, respectively. Furthermore, G_j is given by

$$G_j = \begin{pmatrix} 1 & -\frac{\sigma_j}{\varepsilon_0\omega} \\ 0 & 1 \end{pmatrix}, \tag{8}$$

which we call *conductivity matrix* for the j-th graphene sheet with μ_g-j-th chemical potential. The introduction of the matrix G permit us to maintain the Pochi-Yeh scheme for transfer matrix method [51] under a small modification. The transfer matrix for the

complete system has the form:

$$M = D_0^{-1}[\Pi_{j=1}^{N-1} G_j D_j P_j D_j^{-1}] G_N D_t. \tag{9}$$

Finally, the dispersion relation of plasmonic modes in the graphene-dielectric system is obtained from the poles of reflection via $M_{11} = 0$.

2.2. Plasmonic modes of one and two graphene layers

In the simplest case, a graphene layer is embedded between two dielectric media of relative permittivity ε_0 and ε_t. For this system, an analytic equation for the dispersion relation of graphene plasmonic modes was obtained by Bludov et al. [31], and it is entirely equivalent to get the poles of reflection. The dispersion relation of a single graphene layer is given by

$$\frac{\varepsilon_0}{\kappa_{z0}} + \frac{\varepsilon_t}{\kappa_{zt}} + i\frac{\sigma(\omega)}{\omega\varepsilon_0} = 0, \tag{10}$$

where $\sigma(\omega)$ and κ_{zj} are given by Eqs. (1) and (5), respectively. Real solutions of Eq. (10) are possible only if the imaginary part of conductivity is positive. From Eq. (1), the Drude-like intraband contribution allows for the existence of a single plasmonic mode for one graphene sheet. The interband contribution for this mode will be discussed in subsection 2.3.

When two graphene layers are embedded between three dielectrics media of relative permittivity ε_0, ε_1 and ε_t, previous works have pointed out that the analytic equation for dispersion relation of graphene plasmonic modes can be obtained by

$$\begin{aligned} &e^{\kappa_{1z}d_1}\left(\frac{\varepsilon_0}{\kappa_{0z}} + \frac{\varepsilon_1}{\kappa_{1z}} + i\frac{\sigma}{\omega\varepsilon_0}\right)\left(\frac{\varepsilon_1}{\kappa_{1z}} + \frac{\varepsilon_t}{\kappa_{tz}} + i\frac{\sigma}{\omega\varepsilon_0}\right) = \\ &e^{-\kappa_{1z}d_1}\left(\frac{\varepsilon_0}{\kappa_{0z}} - \frac{\varepsilon_1}{\kappa_{1z}} + i\frac{\sigma}{\omega\varepsilon_0}\right)\left(\frac{\varepsilon_t}{\kappa_{tz}} - \frac{\varepsilon_1}{\kappa_{1z}} + i\frac{\sigma}{\omega\varepsilon_0}\right), \end{aligned} \tag{11}$$

where d_1 is the separation distance between both graphenes, according to our notation (see Fig. 1), and the chemical potentials for the two graphene sheets are the same [31].

When three or more graphene layers are considered in the multi-structure, obtaining the analytic equation for dispersion relation of graphene plasmonic modes can be very cumbersome; therefore the corresponding transcendental equations must be numerically solved. We propose to achieve this task by using the transfer matrix method through the poles of reflectance via $M_{11}(\omega, q_x) = 0$ solutions.

2.3. Asymptotic behavior and interband high frequency mode

We point out in Sec. 1, that many authors refer both intraband and interband contributions in graphene conductivity response, however, when numerical calculations are shown, most of them only take into account the Drude-like intraband contribution. In this section, we analyze the behavior of plasmonic modes for large wavevectors, $q_x \gg (\omega/c)\sqrt{\varepsilon_j}$, therefore $\kappa_{jz} \approx q_x$ and rhs of Eq. (11) is nearly zero. So, Eq. (11) is approximately

$$\left(\frac{\varepsilon_0 + \varepsilon_1}{q_x} + i\frac{\sigma}{\omega\varepsilon_0}\right)\left(\frac{\varepsilon_1 + \varepsilon_t}{q_x} + i\frac{\sigma}{\omega\varepsilon_0}\right) \approx 0. \tag{12}$$

As $(\varepsilon_j + \varepsilon_{j+1})/q_x$ is a non negative term, each independent term of Eq. (12) can be canceled only by a negative term which is possible only if the imaginary part of conductivity is positive. Considering the complete graphene conductivity response as $\sigma = \sigma' + i\sigma''$, where σ' and σ'' are the real and imaginary parts of graphene conductivity, respectively, the domain where

$$\sigma''(\omega) = \frac{e^2|\mu_g|}{\pi\hbar^2\omega} + \frac{e^2}{4\hbar}\frac{1}{2\pi}\ln\left(\frac{\hbar\omega - 2\mu_g}{\hbar\omega + 2\mu_g}\right)^2, \tag{13}$$

is non-negative, allowing for the existence of plasmonic modes for a large wavevectors regimen and it will remain for frequencies below ω_{spp}, where

$$\frac{e^2|\mu_g|}{\pi\hbar^2\omega_{spp}} + \frac{e^2}{4\pi\hbar}\ln\left(\frac{\hbar\omega_{spp} - 2\mu_g}{\hbar\omega_{spp} + 2\mu_g}\right) = 0, \tag{14}$$

which is satisfied when $\hbar\omega_{spp} \cong 1.6671\mu_g$. The condition of Eq. (14) leads to an asymptotic behavior of plasmonic bands.

Now, we shall analyze the existence of an upper mode in the dispersion relation of the graphene-dielectric multilayer system. For $\hbar\omega > 2\mu_g$, the real part of the interband contribution of graphene conductivity response does not vanish.

Taking the approximation of the dispersion relation, Eq. (12), it is necessary to satisfy simultaneously both real and imaginary parts from the equation:

$$\left(\frac{\varepsilon_0 + \varepsilon_1}{q_x} - \frac{\sigma''}{\omega\varepsilon_0}\right)\left(\frac{\varepsilon_1 + \varepsilon_t}{q_x} - \frac{\sigma''}{\omega\varepsilon_0}\right) - \frac{\sigma'^2}{(\omega\varepsilon_0)^2} \approx 0 \tag{15}$$

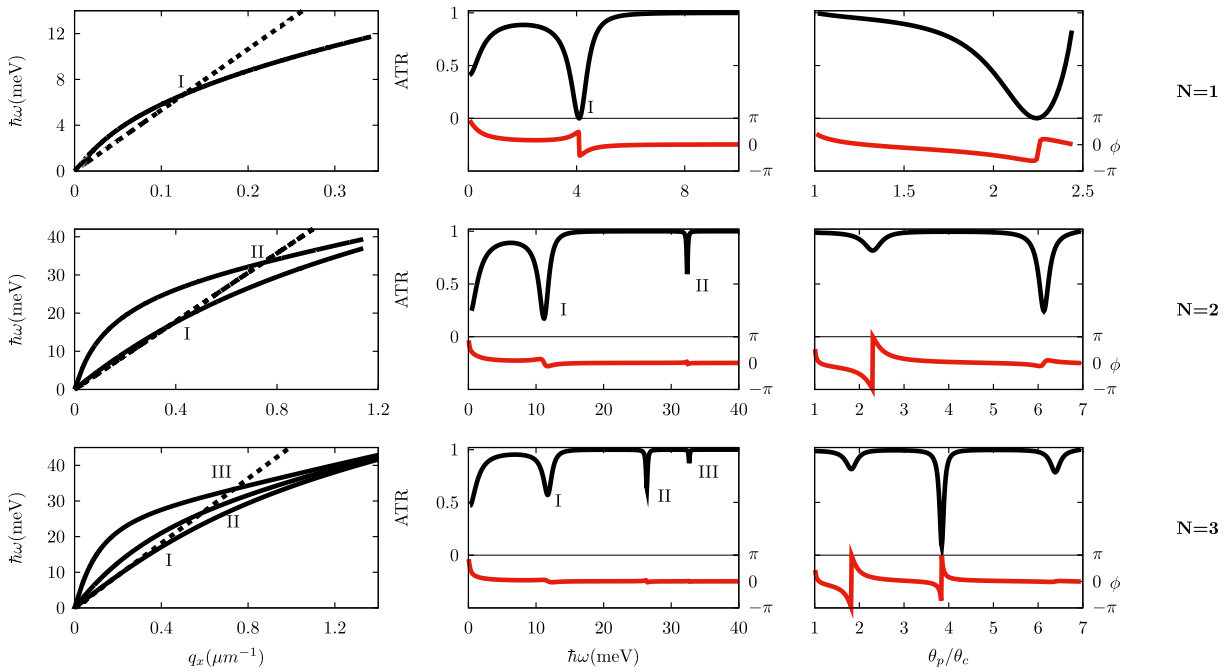

Fig. 2. Left column displays the dispersion relation of graphene SPP calculated for one (N = 1), two (N = 2) and three (N = 3) graphene sheets. Numerals Roman indicate intersection energies of light lines with the SPP branches. ATR spectra and the phase of the reflection coefficient (PCR) as a function of the energy are displayed in the middle columns, for fixed angles (black and red lines, respectively). The right column shows the ATR and the PCR as a function of the incident angle normalized to the critical angle (θ_c), for fixed energies (see text).

$$\frac{(\varepsilon_0 + 2\varepsilon_1 + \varepsilon_t)}{q_x} - \frac{2\sigma''}{\varepsilon_0 \omega} \approx 0 \tag{16}$$

Under $\hbar\omega \gg 2\mu_g$ consideration, $|\sigma'|/|\sigma''|$ is greater than 1. Therefore, we only keep σ' in the first condition of Eq. (15) as

$$\frac{(\varepsilon_0 + \varepsilon_1)(\varepsilon_1 + \varepsilon_t)}{q_x^2} - \frac{\sigma'^2}{(\omega\varepsilon_0)^2} - \approx 0 \tag{17}$$

or

$$\hbar\omega \approx \frac{\pi\alpha}{\sqrt{(\varepsilon_0 + \varepsilon_1)(\varepsilon_1 + \varepsilon_t)}} q_x \hbar c, \tag{18}$$

where $\alpha \approx 1/137$ is the fine structure constant.

This linear equation explains the asymptotic behavior of an upper mode which we show and discuss in the next section.

3. Discussion and results

In order to study the plasmonic modes of a graphene-dielectric multilayer system, we propose the structure showed in Fig. 1. In contrast with previous developed works by Zhan et al., and Bludov et al., where they only show the dispersion relation for one and two graphene sheets [27,31], we show the general case for *N* graphene sheets. Additionally, the ATR in the Otto configuration was calculated as a function of the incidence angle and frequency. Finally, we show that the number of branches in the dispersion relation correspond exactly to the number of graphene sheets in the system, and for the interband region, a superior mode appears.

Fig. 2 shows the dispersion relation, the ATR spectra and the phase of the reflection coefficient (PCR) for one, two, and three graphene sheets. The first, second and third rows correspond to $N = 1,\ 2,\ 3$, respectively. The first column corresponds to the dispersion relation, the second (third) column display the ATR and PCR as a function of the energy (normalized incidence angle). The parameters for the calculation were chosen as follows: $\mu_g = 0.45$ eV and $\Gamma = 0.1$ meV. For one graphene sheet, $\varepsilon_0 = 1$, $\varepsilon_t = 5$, and for $N = 2,3$, $\varepsilon_0 = \varepsilon_t = \varepsilon_j = 1$. The light line in Otto setup given by $k_p = \omega\sqrt{\varepsilon_p}\sin\theta_p/c$ is indicated with the dashed line in Fig. 2. Here, θ_p is the incident angle inside prism and ε_p its permittivity, where $\varepsilon_p = 14$ for the first row and $\varepsilon_p = 20$ for the second and third rows. Intersections of this lines with the dispersion curves correspond to the coupling of the plane waves with the plasmonic modes, i.e., the surface plasmon polaritons in the graphene sheets. The intersection energies for the SPP graphene modes are observed at 4.1 meV for $N = 1$; 12.8 meV and 32.7 meV for $N = 2$; and 11.7 meV, 26.4 meV, and 32.7 meV for $N = 3$ in the ATR spectra (middle column), with θ_p angles fixed to be $2.25\ \arcsin(\sqrt{5/14}) = 82.6°$, $6\ \arcsin(\sqrt{1/20}) = 77.5°$ and $5.9\ \arcsin(\sqrt{1/20}) = 76.2°$, for $N = 1$, 2 and 3 graphene sheets, respectively. In the right column of Fig. 2 we show the ATR spectra as a function of the incident angle for fixed energy values

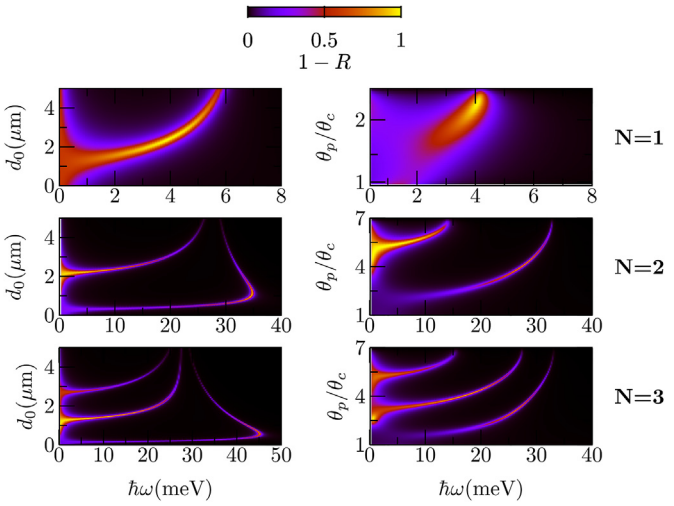

Fig. 3. Left column displays the contour plots of ATR spectra as a function of the frequency and the distance to the prism for one ($N = 1$), two ($N = 2$) and three ($N = 3$) graphene sheets. Right column displays ATR spectra as a function of the frequency and the incident angle normalized to the critical angle.

of $\hbar\omega = 4.1$ meV, 12 meV, and 14.6 meV, for $N = 1, 2$ and 3 graphene sheets, respectively. To keep the total reflection regimen, we must choose $\varepsilon_j < \varepsilon_p$, for any j, and incident angle must lie within the range $\theta_c \leq \theta_p \leq \pi/2$. It can be clearly observed the ATR sharp dips for the different number of graphene sheets, closed to the normal modes energy of SPP (second and third columns, respectively), which allows for both spectral and angular SPP detection. On the other hand, it can be observed that PCR can give complementary information to detect the SPP in graphene, i.e., in the second column we obtain more information about SPP from ATR spectra than PCR, however, in the angular spectra (third column), it is clear that PCR generates a better response as compare to ATR spectra. This behavior suggest that experimentally, the PCR can be employed as an additional technique to detect SPP in graphene due to its high sensitivity [54–58].

In Fig. 3 we show in the first column the ATR contour plots of as a function of the energy versus distance from prism; in the second column it is displayed the ATR contour plots as a function of the energy versus normalized incidence angle. The first, second and third rows correspond to $N = 1, 2, 3$ graphene sheets, respectively. In particular, we can observe that the excitation of SPP can be tuned around the vicinity of the energy or the incidence angle for the normal modes of SPP. Moreover, by selecting the adequate d_0 or θ_p, we can obtain the number of required branches. It is important to highlight that for large distances as well as for sub-micron distances, it is impossible to couple energy to the multi-structure, there are not plasmon excitation in all cases. Therefore, there will be optimum distances and incidence angles which enable us to detect the plasmonic modes. For instance, in the left column of Fig. 3 we can observe that for $N = 2$ and $d_0 = 2.45$ μm two branches can be detected, in contrast to $d_0 = 1$ μm, where only one branch can be detected. In the case of ATR angular resolved, the same procedure can be employed to detect one or two branches (see right column of Fig. 3 for $N = 2$). As we increase the number of graphene-dielectric periods ($N = 3$), it is observed an analogous behavior with the number of branches. On the other hand, by fixing the energy of the incident light, superior modes for different distances are allowed, where we can find coupling modes. We suggest that this behavior is due to light resonant inside the multilayer structure as we observed by increasing the thickness of dielectric layers, where the superior mode is suppressed.

Now, we analyze the multilayer structure for $N = 4$, 6 and 10 graphene sheets suspended in air, i.e., $\varepsilon_j = 1.0$, see Fig. 4. As can be observed, the number of branches of the dispersion relation correspond with the number of graphene sheets; all branches arise from the origin, and they stay in the right of the light line ($q_x = \omega/c$). There is an intermediate region of q_x where the plasmonic modes interact stronger between them, producing a breaking of the initial degeneration of branches. However, when q_x goes to infinity, the modes degenerate again, because it implies that the wavelength is very small and therefore the coupling of the modes disappear. This behavior can also be observed if we change the separation distance d_j of graphene sheets. When d_j is small the modes are not degenerated, however when the distance is larger, the modes degenerate. An important aspect to highlight is the asymptotic value of $\hbar\omega = 1.6671\mu_g$, where all the branches of graphene-dielectric multilayer converge as $q_x \to \infty$. This asymptotic value corresponds with the energy of the surface plasmon supported by one graphene sheet, which has been demonstrated in Eq. (14).

Fig. 5 shows the dispersion relation for two and four graphene sheets including the energy upper to $2\mu_g$, where the interband contribution of graphene conductivity is predominant as compared to Drude contribution. It is well-known that optical and acoustic branches are present below this region, as we discussed above. Additional to these bands, an upper branches emerges, as can be observed in Fig. 5 for higher values of $2\mu_g$.

We fix the separation dimensionless distance between graphenes as $d(\mu_g/\hbar c) = 5 \times 10^{-3}$. For Fig. 5(a), all permittivities are $\varepsilon_j = 1$, and for Fig. 5(b) we consider $\varepsilon_1 = 2.5$. We observe that the upper mode position can be modulated to higher values of q_x wavevector as dielectric permittivities of surrounding media change. We can explain this behavior throughout Eq. (18). The asymptotic slope limits this upper mode and can be changed with the permittivities of surrounding media, showed as dashed line in Fig. 5(a) and (b). We

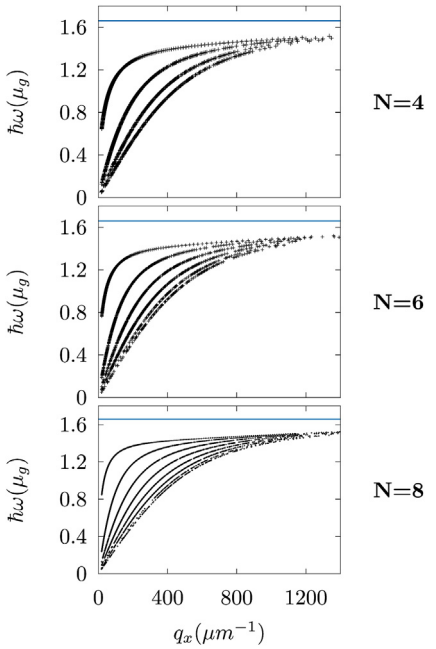

Fig. 4. Dispersion relation of graphene SPP calculated for four (N = 4), six (N = 6) and eight (N = 8) graphene sheets. An asymptotic value of $\hbar\omega = 1.6671\mu_g$ is shown in blue line, where all the branches of graphene-dielectric multilayer converge.

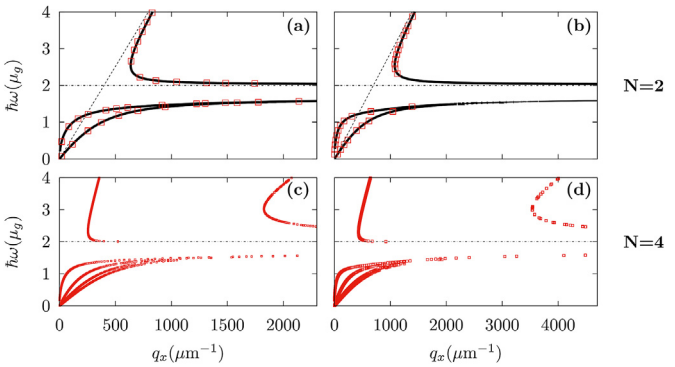

Fig. 5. Dispersion relation showing the upper and lower modes for two (panels (a) and (b)) and four (panels (c) and (d)) graphene sheets, considering the intra and interband contributions of graphene conductivity. Optical and acoustic bands are bounded by the energy $\hbar\omega = 1.667\mu_g$. The upper modes have an horizontal asymptotic value $\hbar\omega_S = 2\mu_g$ (dashed-dotted line) and for N = 2, asymptotic slope (dashed line). Discrete numerical calculation via transfer matrix method of plasmonic modes are indicated with red boxes and black solid line is obtained using the analytic equation (11). Left column corresponds to $\varepsilon_j = 1$ and $d\mu_g/\hbar c = 5 \times 10^{-3}$, right column we change $\varepsilon_2 = 2.5$, and $\varepsilon_{1,3} = 1.5$ (see text).

confirm this upper bands with discrete numerical calculation via transfer matrix method of plasmonic modes, indicated with red boxes. Using the analytic equation Eq. (11), we get the solid black line for the case $N = 2$.

Upper mode for a graphene-dielectric multilayer system with three or more graphene sheets remains, and it is possible to obtain additional upper branches. For Fig. 5(c), we consider four graphene sheets, and all permittivities are equal to $\varepsilon_j = 1$, while for Fig. 5(d) we choose $\varepsilon_0 = \varepsilon_t = 1$, $\varepsilon_1 = \varepsilon_3 = 1.5$, and $\varepsilon_2 = 2.5$. In both cases, we find two upper modes and they can be modulated by modifying the dielectric constants of media where graphene sheets are embedded. The asymptotic behavior of this upper modes remains too. The upper modes for $n \geq 3$ can only be obtained using numerical calculation. To get an analytic close form of these upper modes can be a cumbersome process.

From the dispersion relation obtained in Fig. 5, for upper modes, there will be a propagating mode with positive group velocity. In contrast, for the region close to $\hbar\omega \approx 2\mu_g$, the upper modes have zero nearly negative group velocity. Each upper mode have different asymptotic slope.

Finally, it is important to highlight that upper modes only appear when the interband contribution of conductivity is taken into account.

4. Conclusions

We used the transfer matrix method to calculate numerically the dispersion relation for a graphene-dielectric multilayer system. First, for one, two and three graphene-dielectric sheets we obtain the dispersion relation, and we get ATR spectra, the optimum distance and optimum incident angle to coupling a prism with the multilayer system for detecting the surface plasmon polariton dips in the Otto configuration. We observed that the number of plasmonic branches correspond to the number of graphene sheets in the system for $0 < \hbar\omega < 2\mu_g$ energy range. In all calculations, we took into account both inter and intraband contributions of graphene conductivity response, and for large wavevectors parallel to graphene plane, we found that all plasmonic bands tend to the asymptotic value of energy $\hbar\omega_{spp} = 1.6671\mu_g$, in the non-retarder limit, independent of the number of graphene sheets. We found that for two graphene sheets or more, the dispersion relation shows an upper mode for high frequency associated to interband transition which, to the best of our knowledge, has not been reported before in the literature. For this upper mode for two graphene sheets, we analyzed its asymptotic behavior derived from the analytic dispersion relation.

Acknowledgments

This project is supported by National Council of Science and Technology, Mexico grant no. 259278, PRODEP-SEP (grant UAZ-PTC-199) and Cátedras Conacyt (grant 1577). We acknowledge the technical support provided by Jesús Ernesto Madrigal Sustaita.

Appendix A. Supplementary data

Supplementary data to this article can be found online at https://doi.org/10.1016/j.spmi.2018.11.015.

References

[1] S.A. Maier, Plasmonics: Fundamentals and Applications, Springer, 2007.
[2] J. Zhang, L. Zhang, W. Xu, Surface plasmon polaritons: physics and applications, J. Phys. D Appl. Phys. 45 (2012) 113001https://doi.org/10.1088/0022-3727/45/11/113001.
[3] X. Chen, L.-G. Wang, Propagation of Electron Waves in Monolayer Graphene and Optical Simulations with Negative-zero-positive Index Metamaterials: Physics and Applications of Graphene, InTech, 2011, pp. 1–26 https://doi.org/10.5772/14069.
[4] A. Sommerfeld, Ueber die Fortpflanzung elektrodynamischer Wellen längs eines Drahtes, Ann. Phys. 303 (2) (1899) 233–290, https://doi.org/10.1002/andp.18993030202.
[5] J. Zenneck, Über die Fortpflanzung ebener elektromagnetischer Wellen längs einer ebenen Leiterfläche und ihre Beziehung zur drahtlosen Telegraphie, Ann. Phys. 328 (10) (1907) 846–866 https://doi.org/10.1002/andp.19073281003.
[6] R.W. Wood, XLII. On a remarkable case of uneven distribution of light in a diffraction grating spectrum, London, Edinburgh Dublin Phil. Mag. J. Sci. 4 (21) (1902) 396–402. Taylor & Francis https://doi.org/10.1080/14786440209462857.
[7] V.M. Agranovich, D.L. Mills (Eds.), Surface Polaritons, Notrh-Holland, 1982.
[8] J.M. Pitarke, V.M. Silkin, E.V. Chulkov, P.M. Echenique, Theory of surface plasmons and surface-plasmon polaritons, Rep. Prog. Phys. 70 (1) (2007) 1–87 https://doi.org/10.1088/0034-4885/70/1/R01.
[9] R.H. Ritchie, Plasma losses by fast electrons in thin films, Phys. Rev. 106 (5) (1957) 874–881 https://doi.org/10.1103/PhysRev.106.874.
[10] V. Ryzhii, A. Satou, T. Otsuji, Plasma waves in two-dimensional electron-hole system in gated graphene heterostructures, J. Appl. Phys. 101 (2) (2007), https://doi.org/10.1063/1.2426904.
[11] L.A. Falkovsky, Optical properties of doped graphene layers, J. Exp. Theor. Phys. 106 (3) (2008) 575–580 https://doi.org/10.1134/S1063776108030175.
[12] F. Rana, Graphene terahertz plasmon oscillators, IEEE Trans. Nanotechnol. 7 (1) (2008) 91–99 https://doi.org/10.1109/TNANO.2007.910334.
[13] A. Hill, S.A. Mikhailov, K. Ziegler, Dielectric function and plasmons in graphene, Europhys. Lett. 87 (2) (2009) 27005https://doi.org/10.1209/0295-5075/87/27005.
[14] M. Jablan, H. Buljan, M. Soljačić, Plasmonics in graphene at infrared frequencies, Phys. Rev. B 80 (24) (2009) 1–7 https://doi.org/10.1103/PhysRevB.80.245435.
[15] A.A. Dubinov, V.Y. Aleshkin, V. Mitin, T. Otsuji, V. Ryzhii, Terahertz surface plasmons in optically pumped graphene structures, J. Phys. Condens. Matter 23 (14) (2011) 145302https://doi.org/10.1088/0953-8984/23/14/145302.
[16] L. Ju, B. Geng, J. Horng, C. Girit, M. Martin, Z. Hao, H. a. Bechtel, X. Liang, A. Zettl, Y.R. Shen, F. Wang, Graphene plasmonics for tunable terahertz metamaterials, Nat. Nanotechnol. 6 (10) (2011) 630–634 https://doi.org/10.1038/nnano.2011.146.
[17] F.H. Koppens, D.E. Chang, F.J. García De Abajo, Graphene plasmonics: a platform for strong light-matter interactions, Nano Lett. 11 (8) (2011) 3370–3377 https://doi.org/10.1021/nl201771h.
[18] T.R. Zhan, F.Y. Zhao, X.H. Hu, X.H. Liu, J. Zi, Band structure of plasmons and optical absorption enhancement in graphene on subwavelength dielectric gratings at infrared frequencies, Phys. Rev. B 86 (16) (2012) 2–6 https://doi.org/10.1103/PhysRevB.86.165416.
[19] A.N. Grigorenko, M. Polini, K.S. Novoselov, Graphene plasmonics, Nat. Photon. 6 (2012) 749758https://doi.org/10.1038/NPHOTON.2012.262.
[20] P. Tassin, T. Koschny, M. Kafesaki, C.M. Soukoulis, A comparison of graphene, superconductors and metals as conductors for metamaterials and plasmonics, Nat. Photon. 6 (4) (2012) 259–264 https://doi.org/10.1038/nphoton.2012.27.
[21] T. Stauber, G. Gómez-Santos, Plasmons and near-field amplification in double-layer graphene, Phys. Rev. B 85 (7) (2012) 075410https://doi.org/10.1103/PhysRevB.85.075410.
[22] R.E.V. Profumo, R. Asgari, M. Polini, A.H. MacDonald, Double-layer graphene and topological insulator thin-film plasmons, Phys. Rev. B 85 (8) (2012) 085443https://doi.org/10.1103/PhysRevB.85.085443.
[23] J. Chen, M. Badioli, P. Alonso-González, S. Thongrattanasiri, F. Huth, J. Osmond, M. Spasenović, A. Centeno, A. Pesquera, P. Godignon, A.Z. Elorza, N. Camara, F.J. García de Abajo, R. Hillenbrand, F.H.L. Koppens, Optical nano-imaging of gate-tunable graphene plasmons, Nature 487 (7405) (2012) 77–81 https://doi.org/10.1038/nature11254.
[24] H. Yan, X. Li, B. Chandra, G. Tulevski, Y. Wu, M. Freitag, W. Zhu, P. Avouris, F. Xia, Tunable infrared plasmonic devices using graphene/insulator stacks, Nat. Nanotechnol. 7 (5) (2012) 330–334 https://doi.org/10.1038/nnano.2012.59.
[25] N.M.R. Peres, A. Ferreira, Y.V. Bludov, M.I. Vasilevskiy, Light scattering by a medium with a spatially modulated optical conductivity: the case of graphene, J. Phys. Condens. Matter 24 (24) (2012) 245303https://doi.org/10.1088/0953-8984/24/24/245303.
[26] C. How Gan, Analysis of surface plasmon excitation at terahertz frequencies with highly doped graphene sheets via attenuated total reflection, Appl. Phys. Lett. 101 (11) (2012) 111609https://doi.org/10.1063/1.4752465.
[27] T. Zhan, X. Shi, Y. Dai, X. Liu, J. Zi, Transfer matrix method for optics in graphene layers, J. Phys. Condens. Matter 25 (21) (2013) 215301https://doi.org/10.

1088/0953-8984/25/21/215301.
[28] Y.V. Bludov, N.M.R. Peres, M.I. Vasilevskiy, Unusual reflection of electromagnetic radiation from a stack of graphene layers at oblique incidence, J. Optic. 15 (11) (2013) 1–13 https://doi.org/10.1088/2040-8978/15/11/114004.
[29] N.M. Peres, Y.V. Bludov, A. Ferreira, M.I. Vasilevskiy, Exact solution for square-wave grating covered with graphene: surface plasmon-polaritons in the terahertz range, J. Phys. Condens. Matter 25 (12) (2013) 125303https://doi.org/10.1088/0953-8984/25/12/125303.
[30] M. Jablan, M. Soljacic, H. Buljan, Plasmons in graphene: fundamental properties and potential applications, Proc. IEEE 101 (7) (2013) 1689–1704 https://doi.org/10.1109/JPROC.2013.2260115.
[31] Y.V. Bludov, A. Ferreira, N.M.R. Peres, M.I. Vasilevskiy, A primer on surface plasmon-polaritons in graphene, Int. J. Mod. Phys. B 27 (10) (2013) 1341001https://doi.org/10.1142/S0217979213410014.
[32] Z. Fang, S. Thongrattanasiri, A. Schlather, Z. Liu, L. Ma, Y. Wang, M. Pulickel Ajayan, P. Nordlander, N.J. Halas, F.J. García De Abajo, Gated tunability and hybridization of localized plasmons in nanostructured graphene, ACS Nano 7 (3) (2013) 2388–2395 https://doi.org/10.1021/nn3055835.
[33] W. Gao, G. Shi, Z. Jin, J. Shu, Q. Zhang, R. Vajtai, P.M. Ajayan, J. Kono, Q. Xu, Excitation and active control of propagating surface plasmon polaritons in graphene, Nano Lett. 13 (8) (2013) 3698–3702 https://doi.org/10.1021/nl401591k.
[34] H. Buljan, M. Jablan, M. Soljačić, Damping of plasmons in graphene, Nat. Photon. 7 (2013) 394399 https://doi.org/10.1038/nphoton.2013.57.
[35] T. Low, P. Avouris, Graphene plasmonics for terahertz to mid-infrared applications, ACS Nano 8 (2) (2014) 1086–1101 https://doi.org/10.1021/nn406627u.
[36] T. Stauber, Plasmonics in Dirac systems: from graphene to topological insulators, J. Phys. Condens. Matter 26 (2014) 123201https://doi.org/10.1088/0953-8984/26/12/123201.
[37] Y.V. Bludov, D.A. Smirnova, Y.S. Kivshar, N.M. Peres, M.I. Vasilevskiy, Nonlinear TE-polarized surface polaritons on graphene, Phys. Rev. B 89 (3) (2014) 035406https://doi.org/10.1103/PhysRevB.89.035406.
[38] P. Avouris, M. Freitag, Graphene photonics, plasmonics, and optoelectronics, IEEE J. Sel. Top. Quant. Electron. 20 (1) (2014) 72–83 https://doi.org/10.1109/JSTQE.2013.2272315.
[39] D.R. Mason, S.G. Menabde, N. Park, Unusual Otto excitation dynamics and enhanced coupling of light to TE plasmons in graphene, Optic Express 22 (1) (2014) 847 https://doi.org/10.1364/OE.22.000847.
[40] F.J.G. De Abajo, Graphene plasmonics: challenges and opportunities, ACS Photonics 1 (3) (2014) 133–152 https://doi.org/10.1021/ph400147y.
[41] Y. Cai, J. Zhu, Q.H. Liu, Tunable enhanced optical absorption of graphene using plasmonic perfect absorbers, Appl. Phys. Lett. 106 (4) (2015) 043105https://doi.org/10.1063/1.4906996.
[42] F. Ramos-Mendieta, Mid-infrared Otto excitation of transverse electric modes in doped graphene, J. Appl. Phys. 117 (13) (2015) 133101https://doi.org/10.1063/1.4916721.
[43] S. Xiao, X. Zhu, B.-H. Li, N.A. Mortensen, Graphene-plasmon polaritons: from fundamental properties to potential applications, Front. Physiol. 11 (2016) 117801https://doi.org/10.1007/s11467-016-0551-z.
[44] A. Dey, A. Chroneos, N.S.J. Braithwaite, R.P. Gandhiraman, S. Krishnamurthy, Plasma engineering of graphene, Appl. Phys. Rev. 3 (2) (2016) 021301–1 https://doi.org/10.1063/1.4947188.
[45] S. Huang, C. Song, G. Zhang, H. Yan, Graphene plasmonics: physics and potential applications, Nanophotonics 6 (6) (2016) 1191–1204 https://doi.org/10.1515/nanoph-2016-0126.
[46] P. Alonso-González, A.Y. Nikitin, Y. Gao, A. Woessner, M.B. Lundeberg, A. Principi, N. Forcellini, W. Yan, S. Vélez, A.J. Huber, K. Watanabe, T. Taniguchi, F. Casanova, L.E. Hueso, M. Polini, J. Hone, F.H.L. Koppens, R. Hillenbrand, Acoustic terahertz graphene plasmons revealed by photocurrent nanoscopy, Nat. Nanotechnol. 12 (1) (2016) 31–35 https://doi.org/10.1038/nnano.2016.185.
[47] A. Politano, I. Radović, D. Borka, Z.L. Mišković, G. Chiarello, Interband plasmons in supported graphene on metal substrates: theory and experiments, Carbon 96 (2016) 91–97 https://doi.org/10.1016/j.carbon.2015.09.053.
[48] K.V. Sreekanth, S. Zeng, J. Shang, K.-T. Yong, T. Yu, Excitation of surface electromagnetic waves in a graphene-based Bragg grating, Sci. Rep. 2 (1) (2012) 737 https://doi.org/10.1038/srep00737.
[49] K. Jamalpoor, A. Zarifkar, M. Miri, Application of graphene second-order nonlinearity in THz plasmons excitation, Photonics Nanostruct. 26 (2017) 80–84 https://doi.org/10.1016/j.photonics.2017.08.002.
[50] F. Wang, Y. Zhang, C. Tian, C. Girit, A. Zettl, M. Crommie, Y.R. Shen, Gate-variable optical transitions in graphene, Science 320 (5873) (2008) 206–209 https://doi.org/10.1126/science.1152793.
[51] P. Yeh, Optical Waves in Layered Media, Wiley Inter-Science, 2005.
[52] P. Markos, C.M. Soukoulis, Wave Propagation: from Electrons to Photonic Crystals and Left-handed Materials, Princenton University Press, 2008.
[53] L.A. Falkovsky, Optical properties of graphene, J. Phys. Conf. 129 (1) (2008) 012004https://doi.org/10.1088/1742-6596/129/1/012004.
[54] S.G. Nelson, K.S. Johnston, S.S. Yee, High sensitivity surface plasmon resonance sensor based on phase detection, Sensor. Actuator. B Chem. 36 (2) (1996) 187–191 https://doi.org/10.1016/S0925-4005(97)80052-4.
[55] V.E. Kochergin, A.A. Beloglazov, M.V. Valeiko, P.I. Nikitin, Phase properties of a surface-plasmon resonance from the viewpoint of sensor applications, Quant. Electron. 28 (5) (1998) 444–448 https://doi.org/10.1070/QE1998v028n05ABEH001245.
[56] S. Deng, P. Wang, X. Yu, Phase-sensitive surface plasmon resonance sensors: recent progress and future prospects, Sensors (Switzerland) 17 (12) (2017) 2819, https://doi.org/10.3390/s17122819.
[57] G. Lan, S. Liu, X. Zhang, Highly sensitive and wide-dynamic-range liquid-prism surface plasmon resonance refractive index sensor based on the phase and angular interrogations, Chin. Optic Lett. 14 (2) (2016) 022401, , https://doi.org/10.3788/COL201614.022401.
[58] S. Mohammadzadeh-Asl, A. Keshtkar, J. Ezzati Nazhad Dolatabadi, M. de la Guardia, Nanomaterials and phase sensitive based signal enhancment in surface plasmon resonance, Biosens. Bioelectron. 110 (2018) 118–131 https://doi.org/10.1016/j.bios.2018.03.051.